RSC Advances

PAPER

View Article Online
View Journal | View Issue

Cite this: *RSC Adv.*, 2019, **9**, 25750

Synthesis of a well-dispersed $CaFe_2O_4$/g-C_3N_4/CNT composite towards the degradation of toxic water pollutants under visible light†

Fei Liu, *[a] Shaocan Dong,[a] Zhaoxiang Zhang,[b] Xiaqing Li,[c] Xiaodong Dai,[a] Yanping Xin,[a] Xuewu Wang,[a] Kun Liu,[a] Zhenhe Yuan[a] and Zheng Zheng[a]

Herein, we fabricated a ternary photocatalyst composed of $CaFe_2O_4$, multiwalled carbon nanotubes (CNTs) and graphitic carbon nitride (g-C_3N_4) *via* a simple hydrothermal route. $CaFe_2O_4$ acted as a photosensitizer medium and the CNT acted as a co-catalyst, which remarkably enhanced the photocatalytic performances of g-C_3N_4 towards the degradation of hexavalent chromium (Cr(VI)) and the antibiotic tetracycline (TC) under visible light irradiation. To investigate the morphological and topological features of the photocatalyst, field-emission scanning electron microscopy (FE-SEM) and transmission electron microscopy (TEM) analyses were performed. The surface properties and oxidation state of the $CaFe_2O_4$/g-C_3N_4/CNT composite were determined by X-ray photoelectron spectroscopy (XPS). The recombination rate of the charge carriers and the band gap values of the as-synthesized catalysts were analyzed by photoluminescence spectroscopy (PL) and diffused reflectance spectroscopy (UV/Vis DRS) studies, respectively. Besides the degradation reactions, the high hydrogen production rate of 1050 μmol h^{-1} under visible light using the $CaFe_2O_4$/g-C_3N_4/CNT composite loaded with 5 wt% CNT was observed. The superior photocatalytic performances of the $CaFe_2O_4$/g-C_3N_4/CNT composite can be ascribed to the effective heterojunction formed between g-C_3N_4 and the $CaFe_2O_4$ matrix, in which the CNT act as a conducting bridge in the system, promoting the production of photoinduced charge carriers in the semiconductor system. Finally, the plausible photocatalytic mechanism towards the degradation of pollutants and hydrogen production was discussed carefully.

Received 2nd July 2019
Accepted 30th July 2019

DOI: 10.1039/c9ra05005a

rsc.li/rsc-advances

1. Introduction

In the past few decades, the reckless release of organic pollutants in water bodies has increased greatly, which cause severe environmental problems and health risks.[1,2] Accordingly, the photocatalysis process using semiconductor photocatalysts has been proposed as a green technology to degrade the organic pollutants in water bodies, even at trace levels.[3] Thus, semiconductor materials, such as TiO_2, SnO_2, and ZnO, have been investigated by various researchers owing to their low cost and ease of availability.[4] However, their foremost drawbacks are their wide band gap energy, high recombination, and low visible light response, which limit their large-scale production in industry.

Recently, a polymeric semiconductor, g-C_3N_4, has emerged with visible light response, excellent quantum efficiency and photochemical stability, presenting a competitive candidate for the degradation of dyes, NO_x removal, CO_2 reduction, and water-splitting reactions.[5] Unfortunately, the pure g-C_3N_4 semiconductor exhibits a sluggish performance due to its high recombination rate and poor absorption ability in the entire visible light region. Furthermore, its low quantum efficiency and turnover number (TON) are also considered a major obstacle.[6] Thus, tremendous efforts have been made to resolve these problems, and a system mainly composed of well-matched semiconductors will be a good way to overcome these issues.[7] The heterojunction between highly visible light active semiconductors with suitable band gap values is favorable for enhanced charge separation efficiency in g-C_3N_4 and dramatically enhances its light absorption ability in the entire visible region.[8]

Thus, calcium ferrite ($CaFe_2O_4$), as p-type visible light-active photocatalyst, has been investigated due to its low cost and toxicity with narrow band gap energy towards the degradation of pollutants in both the gaseous and liquid phase.[9] Nevertheless, its major drawbacks such as inefficient hole transfer property, high recombination rate, and charge mobility result in

[a]*Shengli College, China University of Petroleum, Dongying, Shandong, 257061, China. E-mail: lf88888888lz@sina.com*

[b]*Shengli Oilfield Company Postdoctoral Research Station, Sinopec, Dongying, Shandong, 257000, China*

[c]*Petroleum Engineering Technology Research Institute of Shengli Oilfield Company, SINOPEC, Dongying, Shandong, 257000, China*

† Electronic supplementary information (ESI) available. See DOI: 10.1039/c9ra05005a

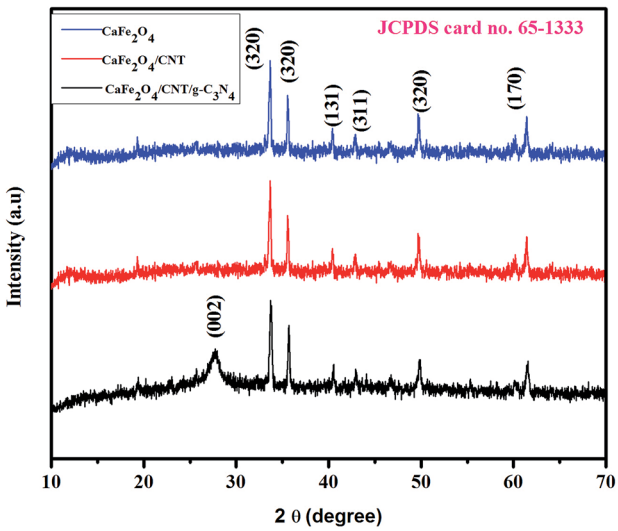

Fig. 1 XRD patterns of the as-prepared $CaFe_2O_4$ and $CaFe_2O_4$/g-C_3N_4/CNT composite.

a sluggish performance.[10] Therefore, the $CaFe_2O_4$ photocatalysts suffered severely during water-splitting reactions and the degradation of pollutants. To solve these issues, Luo *et al.* developed a novel $CaFe_2O_4/Bi_2O_3$ composite *via* a simple wet chemical route. The photocatalytic properties of the $CaFe_2O_4/Bi_2O_3$ composite was evaluated through the degradation of malachite green (MG) dye under visible light irradiation.[11] The higher photocatalytic efficiency can be attributed due to the improved separation of photogenerated electron–hole pairs through the incorporation of Bi_2O_3, which can be beneficial for a higher degradation performance. Liu *et al.* prepared a carbon-modified $CaFe_2O_4$ composite towards the degradation of methylene blue dye.[12] The presence of carbon in $CaFe_2O_4$ greatly influenced the degradation rate of $CaFe_2O_4$ due to its excellent adsorption behavior.

Therefore, it is essential to develop simple and cost-effective methods to improve the photocatalytic ability of both $CaFe_2O_4$ and g-C_3N_4 without sacrificing their crystalline nature and structural stability. CNT are outstanding 1D nano-sized materials with abundant surface hydroxyl and carboxyl groups, which enable their solubility in polar solvents.[13] Thus, anchoring CNT on the surface of $CaFe_2O_4$ and g-C_3N_4 can lead to a superior performance than that of the $CaFe_2O_4$ and g-C_3N_4 binary system. Besides, CNT exhibit a high specific surface area, excellent electron transfer ability, and can act as a noble metal-free co-catalyst in heterojunction systems.[14] The CNT-enabled heterojunction system can afford extra active sites for the adsorption of target pollutants in degradation reactions. Inspired by this mechanism and to further improve the photo-degradation efficiency of both $CaFe_2O_4$ and g-C_3N_4, herein, we demonstrate a simple method for the development of a ternary photocatalyst.[15] Upon the incorporation of CNT, the photocatalytic efficiency was significantly improved towards the hydrogen evolution reaction, and Cr(VI) and TC degradation to a great extent.

2. Experimental

2.1. Materials

All the chemicals used in this work were of analytical reagent (AR) grade. Dicyandiamide, melamine ($C_3H_6N_6$), calcium nitrate tetrahydrate ($Ca(NO_3)_2 \cdot 4H_2O$), iron(III) nitrate nonahydrate ($Fe(NO_3)_3 \cdot 9H_2O$), potassium dichromate, tetracycline hydrochloride, glycerol, ethylene glycol, citric acid, ethanol, methanol and MWCNT were obtained from Sigma-Aldrich Corporation. Deionized (DI) was used throughout the synthesis and photocatalytic process.

2.2. Preparation of g-C_3N_4

g-C_3N_4 was prepared *via* a simple calcination route. In a typical synthesis, a stoichiometric amount of dicyandiamide and melamine (1 : 1 ratio) was added to a silica crucible and calcined at 550 °C for 4 h under a nitrogen atmosphere. Finally, the silica crucible was cooled naturally to obtain porous g-C_3N_4 sheets.

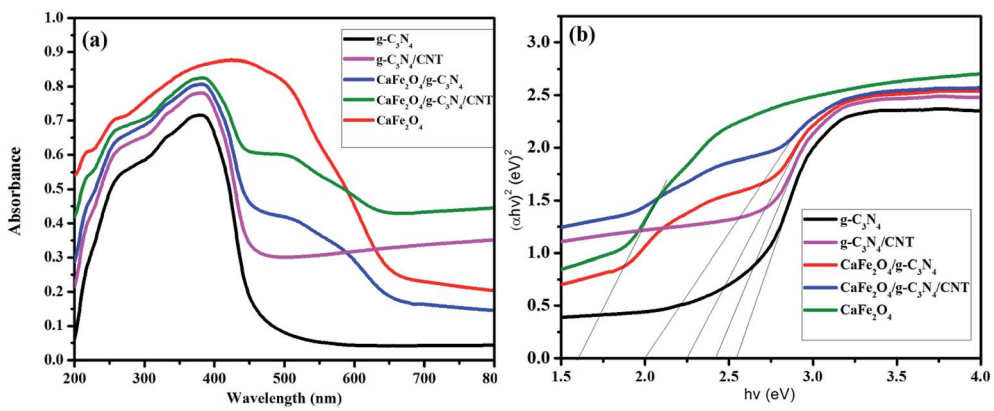

Fig. 2 (a) UV-vis diffuse reflectance spectra of $CaFe_2O_4$, g-C_3N_4, g-C_3N_4/CNTs, and $CaFe_2O_4$/g-C_3N_4/CNT composite. (b) Optical band gap energy, E_g, of $CaFe_2O_4$, g-C_3N_4, g-C_3N_4/CNTs, and $CaFe_2O_4$/g-C_3N_4/CNT composite.

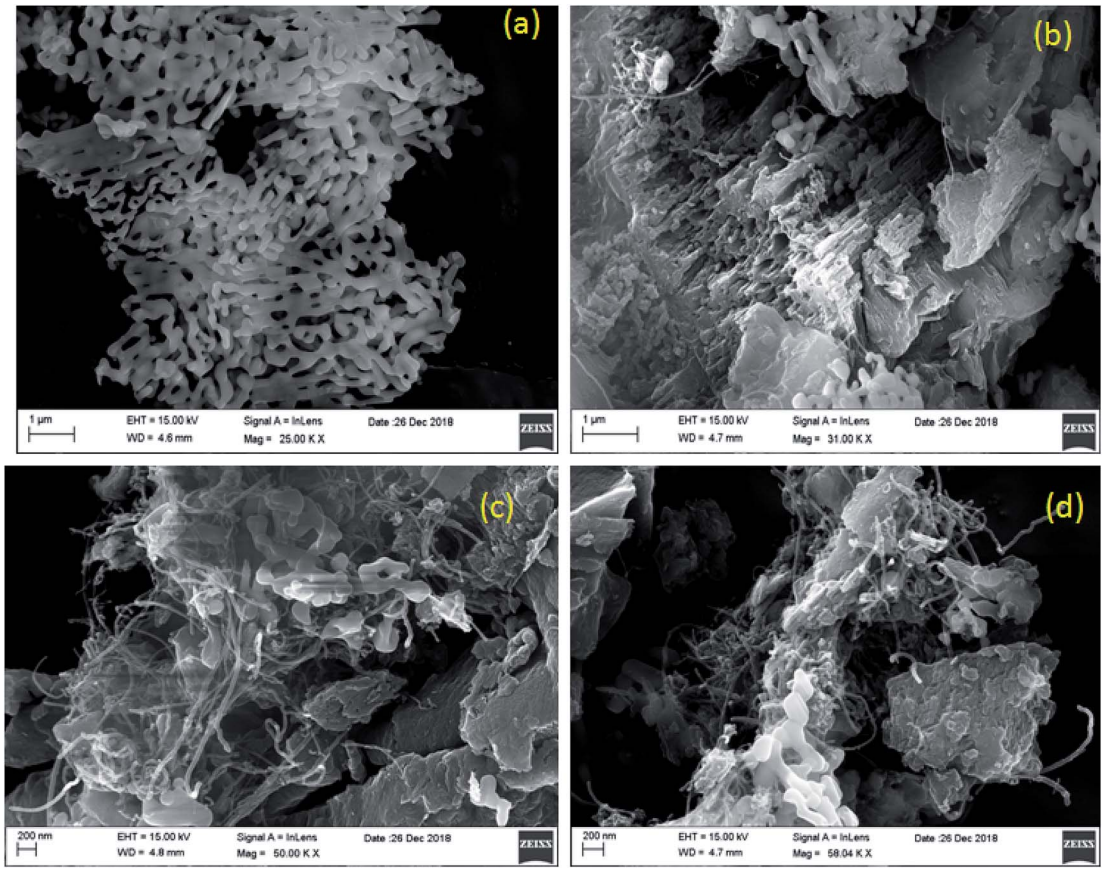

Fig. 3 (a–d) FE-SEM images of $CaFe_2O_4$ and $CaFe_2O_4$/g-C_3N_4/CNT composite.

2.3. Preparation of $CaFe_2O_4$

$CaFe_2O_4$ was synthesized as follows method: a calculated amount of $Ca(NO_3)_2 \cdot 4H_2O$, $Fe(NO_3)_3 \cdot 9H_2O$, glycerol, ethylene glycol, and citric acid was mixed under ultrasound irradiation and stirred for 1 h at 80 °C. The obtained red color fluffy product was further calcined at 850 °C for 3 h under an air atmosphere to obtain the pure-phase $CaFe_2O_4$.

2.4. $CaFe_2O_4$/g-C_3N_4/CNTs composite

A simple hydrothermal route was adopted to synthesize the $CaFe_2O_4$/g-C_3N_4/CNT composite. Typically, the CNT and as-synthesized g-C_3N_4 were dispersed in 20 mL of DI water with the help of ultrasonication for 2 h. Then, a calculated weight percentage of $CaFe_2O_4$ powder was mixed with the above solution and transferred to a Teflon-lined autoclave, which was heated at 120 °C for 12 h. The final brown-colored precipitate was washed with DI water repeatedly and vacuum dried at 70 °C overnight.

2.5. Characterization

The $CaFe_2O_4$/g-C_3N_4/CNT composite was analyzed *via* X-ray diffraction (XRD) on a PANalytical X-ray diffractometer using CuKα radiation ($\lambda = 1.5418$ Å) in the 2θ range of 10–70°. The elemental purity and surface properties of the $CaFe_2O_4$/g-C_3N_4/CNT composite was examined *via* X-ray photoelectron spectroscopy (XPS) on an ESCALAB X-ray photoelectron spectrometer using MgKα radiation. The morphology and microstructures of the prepared samples were recorded *via* TEM (Tecnai G2 F20 transmission electron microscope), and field-emission scanning electron microscopy using an EM, Quanta FEG 250. UV-Vis diffuse reflectance spectra (DRS) of the samples were analyzed an a UV/Vis spectrophotometer (Jasco-V750 Japan) in the wavelength range of 200–900 nm using $BaSO_4$ as an internal standard. Photoluminescence (PL) spectra were measured using a fluorescence spectrophotometer (F-7000, Japan).

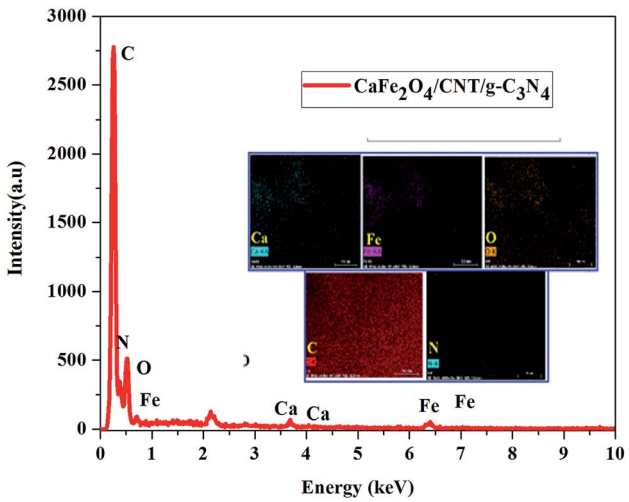

Fig. 4 EDS and elemental mapping analysis of the $CaFe_2O_4$/g-C_3N_4/CNT composite.

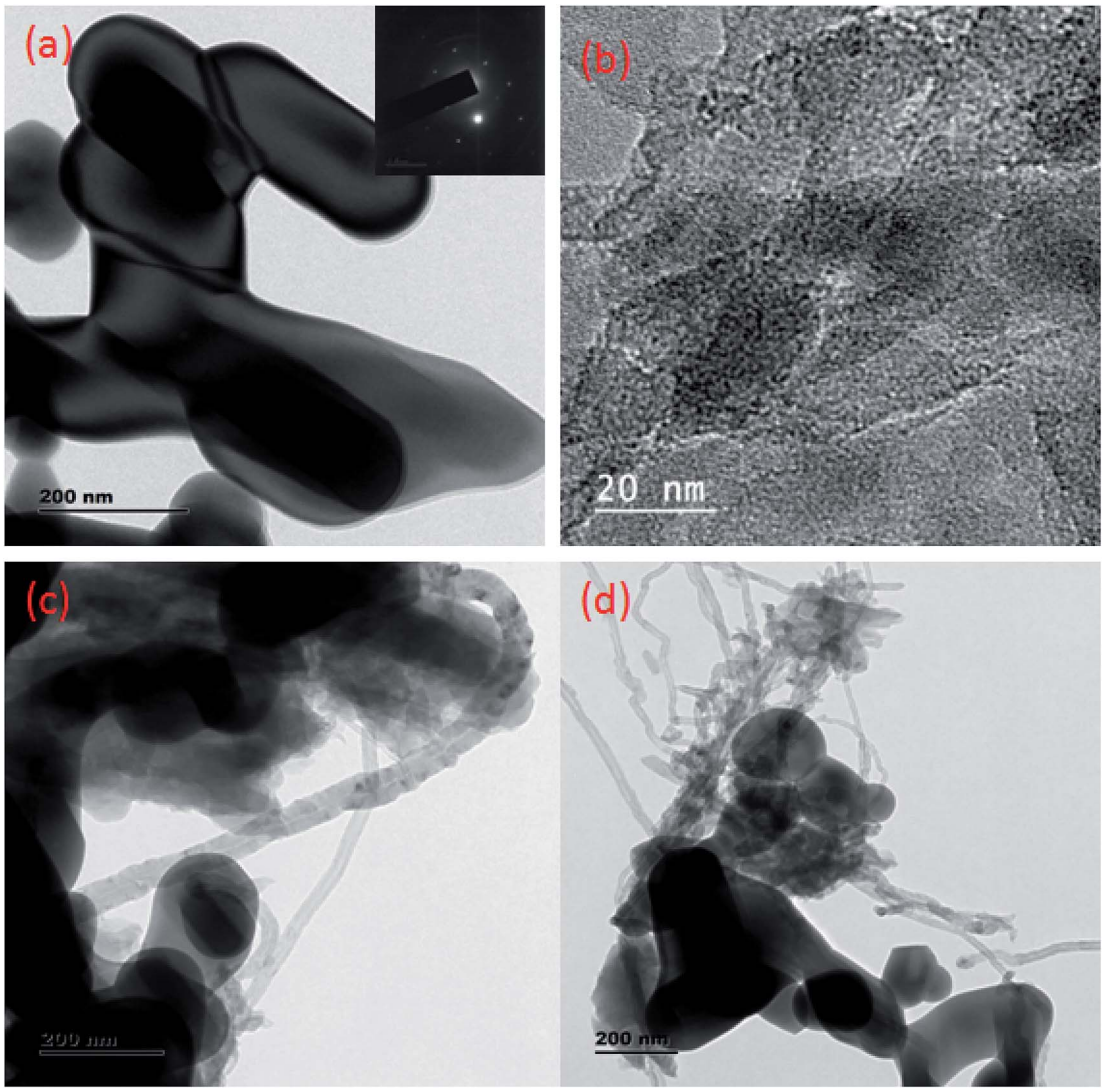

Fig. 5 (a) TEM images of $CaFe_2O_4$ (b) g-C_3N_4 and (c and d) $CaFe_2O_4$/g-C_3N_4/CNT composite.

2.6. Photocatalytic degradation reactions

The aqueous phase degradation of Cr(VI) and TC was performed in a quartz reactor under visible light irradiation ($\lambda \geq 420$ nm) generated by a 300 W Xe lamp. The distance between the test solution and the lamp was fixed at 15 cm. In the degradation process, 0.1 g of powdered photocatalyst was mixed in 100 mL of Cr(VI) and TC with a concentration of 10 ppm. Before visible light irradiation, the suspension was kept in the dark with constant stirring for 20 min to attain equilibrium between the pollutants and photocatalyst. Subsequently, the degraded suspension was collected at given time periods and the absorbance maxima were analyzed by a UV-vis spectrophotometer.

2.7. Photocatalytic H_2 evolution reactions

To measure the hydrogen production rate, the following procedure was adopted. Exactly 50 mg of $CaFe_2O_4$/g-C_3N_4/CNT composite was dispersed in 75 mL of 15 vol% lactic acid solution, and then purged with N_2 for 30 min to remove the oxygen in the reactor vessel. A 4 W LED was applied as the visible-light source and continuous stirring was maintained to keep the photocatalyst suspended in the medium. The amount of hydrogen produced was measured by a gas chromatograph with a TCD detector. The AQY of the $CaFe_2O_4$/g-C_3N_4/CNTs was calculated using the following equation:

$$\text{AQY}\% = \frac{\text{no. of evolved hydrogen molecules} \times 2}{\text{no. of incident photons}} \times 100$$

3. Results and discussion

Fig. 1 shows the XRD patterns of g-C_3N_4, $CaFe_2O_4$, and $CaFe_2O_4$/g-C_3N_4/CNT composite. Two apparent distinguishing peaks of g-C_3N_4 appeared at the 2θ values of 13.1° and 27.8°, which can be perfectly matched with the JCPDS card number 87-1526.[16] All the peaks of $CaFe_2O_4$ correspond to the orthorhombic crystal phase and matched the standard card (JCPDS 32-0168).[17] The

strong interference peak of g-C_3N_4 at 27.5 was observed in the $CaFe_2O_4$/g-C_3N_4/CNT composite, confirming the successful formation of the heterojunction. Furthermore, the characteristic peaks of the CNT were not observed in the system, which can be attributed to their low concentration and poor crystallinity. Thus, the optical properties of the as-synthesized catalyst samples were recorded by UV-vis DRS analysis. Fig. 2a presents the typical UV-vis DRS spectrum of g-C_3N_4, $CaFe_2O_4$ and $CaFe_2O_4$/g-C_3N_4/CNT composite. It can be observed that the absorption maximum of $CaFe_2O_4$ is about 466 nm, while the pure g-C_3N_4 exhibits poor visible light absorption about 470 nm. From the Tauc plot, the band gap energies of $CaFe_2O_4$ and g-C_3N_4 were calculated to be 1.55 eV and 2.57 eV, respectively. Comparing the absorption maxima of g-C_3N_4, g-C_3N_4/CNT and g-C_3N_4/$CaFe_2O_4$ nanocomposites, the $CaFe_2O_4$/g-C_3N_4/CNT composite exhibited a significant red shift with the characteristic absorption edge at 585 nm and band gap energy of 2.02 eV, as shown in Fig. 2b. This may be attributed to the successful formation of an active heterojunction between the g-C_3N_4 and $CaFe_2O_4$ interface and strong electron conducting nature of CNT.[18] Moreover, the enhanced visible light absorption confirmed that the $CaFe_2O_4$/g-C_3N_4/CNT composite can absorb the visible light effectively, which is favorable for the production of hydrogen and degradation of pollutants.[19]

The morphologies of the as-synthesized composites were analyzed by FE-SEM and TEM analysis. The SEM images in Fig. 3a–d show the morphology and structure of $CaFe_2O_4$ and the $CaFe_2O_4$/g-C_3N_4/CNT composite. Fig. 3a shows that the $CaFe_2O_4$ particles are well-dispersed with an average size of 200–300 nm.[20] Fig. 3b–d show the FE-SEM images of the $CaFe_2O_4$/g-C_3N_4/CNT composite, which contains $CaFe_2O_4$, CNT and g-C_3N_4 nanosheets, respectively. Furthermore, the FE-SEM images reveal that g-C_3N_4 exhibited a porous structure with few aggregations. The tube-like CNT were interlinked effectively on the surface of the g-C_3N_4 and $CaFe_2O_4$ matrices.[21] The existence of this heterojunction was further confirmed by the representative elemental mapping images (EDS) in Fig. 4, which show an even distribution of carbon (C), nitrogen (N), calcium (a), oxygen (O) and iron (Fe).

Further, to investigate the microstructure of the obtained samples, TEM characterization was performed. Fig. 5a–d present the typical TEM images of $CaFe_2O_4$, g-C_3N_4, and the $CaFe_2O_4$/g-C_3N_4/CNT composite. For the composite, grey part can be assigned to the sheet-like g-C_3N_4, and the dark particles can be assigned to $CaFe_2O_4$ nanoparticles, which were dispersed effectively on the exterior surface of g-C_3N_4.[22] Furthermore, the TEM images display the existence of a heterojunction stuck between g-C_3N_4 and $CaFe_2O_4$, and the tubular CNT acting as a connecting bridge between these materials. In the SAED patterns, the lattice fringes have a spacing of 0.231 nm, which is consistent with the (131) planes of $CaFe_2O_4$ (JCPDS 32-0168). Thus, these results are in accordance with the XRD analysis. Upon further analysis of the HRTEM images, as shown in Fig. 6, close contact interfaces between $CaFe_2O_4$, g-C_3N_4 and CNT were observed. From the TEM results, it can be concluded that an apparent interface was formed between the g-C_3N_4, CNT, and $CaFe_2O_4$ matrices. Therefore this ternary $CaFe_2O_4$/g-C_3N_4/CNT composite is promising for the transport of charge carriers towards the degradation of Cr(VI) and TC.[23]

The chemical binding energies and oxidation states of the $CaFe_2O_4$/g-C_3N_4/CNT composite were confirmed by XPS (Fig. 7), which was also used to study the valence state properties of the semiconductors. Fig. 7a displays the XPS survey spectrum of the $CaFe_2O_4$/g-C_3N_4/CNT composite. The major peaks of the Ca, Fe, O, C and N elements appeared in the XPS spectra. Fig. 7b displays the elemental scan of the Ca 2p element, where the major peaks at 346.4 eV and 350.2 eV correspond to the Ca $2p_{3/2}$ and Ca $2p_{1/2}$ spins, respectively.[24] The elemental XPS spectrum of Fe 2p in Fig. 7c mainly shows peaks at 710.8 eV and 724.8 eV, representing the Fe $2p_{3/2}$ and Fe $2p_{1/2}$ spins, which indicate the oxidation of Fe was 3+ in $CaFe_2O_4$.[25] The O 1s spectrum in Fig. 7d was deconvoluted into two main peaks at 529.7 eV and 531.8 eV, corresponding to the lattice oxygen in ferrites and surface-adsorbed OH groups, respectively.[26] The C 1s peaks of the composite were located at 288.6 eV and 284.5 eV, which correspond to the C–N and C–C hybridization in the carbon matrix, respectively (Fig. 7e). The peaks observed at 398.7 eV and 398.5 eV are attributed to the sp^2-hybridized nitrogen atoms in the triazine rings. Furthermore, the sharp peak observed at 401.4 eV corresponds to the strong binding of nitrogen with carbon atoms such as N–$(C)_3$ (Fig. 7f).[27] Thus, the structural analysis with XRD, FE-SEM, TEM, UV-vis DRS, and XPS suggests that the $CaFe_2O_4$/g-C_3N_4/CNT composite was successfully synthesized.

It is worth mentioning that highly proficient visible light-active photocatalytic reactions are mainly a result of fast separation efficiency, good redox reactions and high visible light absorption.[28] The electron–hole separation and charge transfer properties of g-C_3N_4 and the $CaFe_2O_4$/g-C_3N_4/CNT composite was confirmed by PL analysis, and the data is shown in Fig. 8. g-C_3N_4 showed the highest PL peak intensity, which confirms that

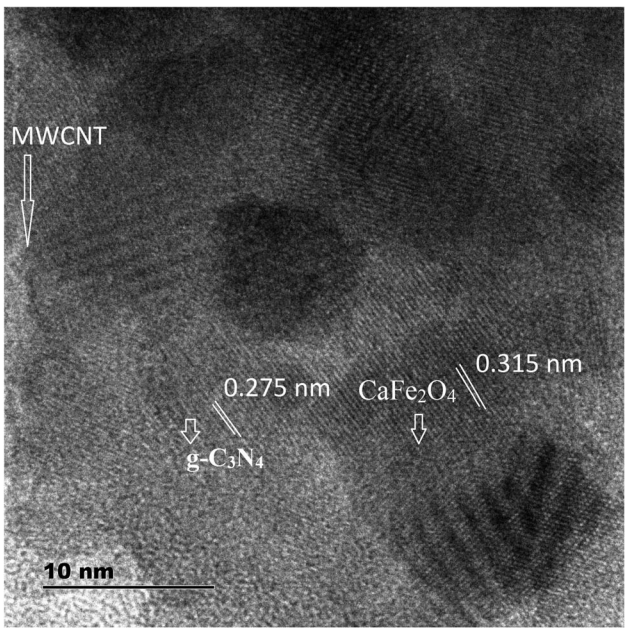

Fig. 6 HRTEM images of the $CaFe_2O_4$/g-C_3N_4/CNT composite.

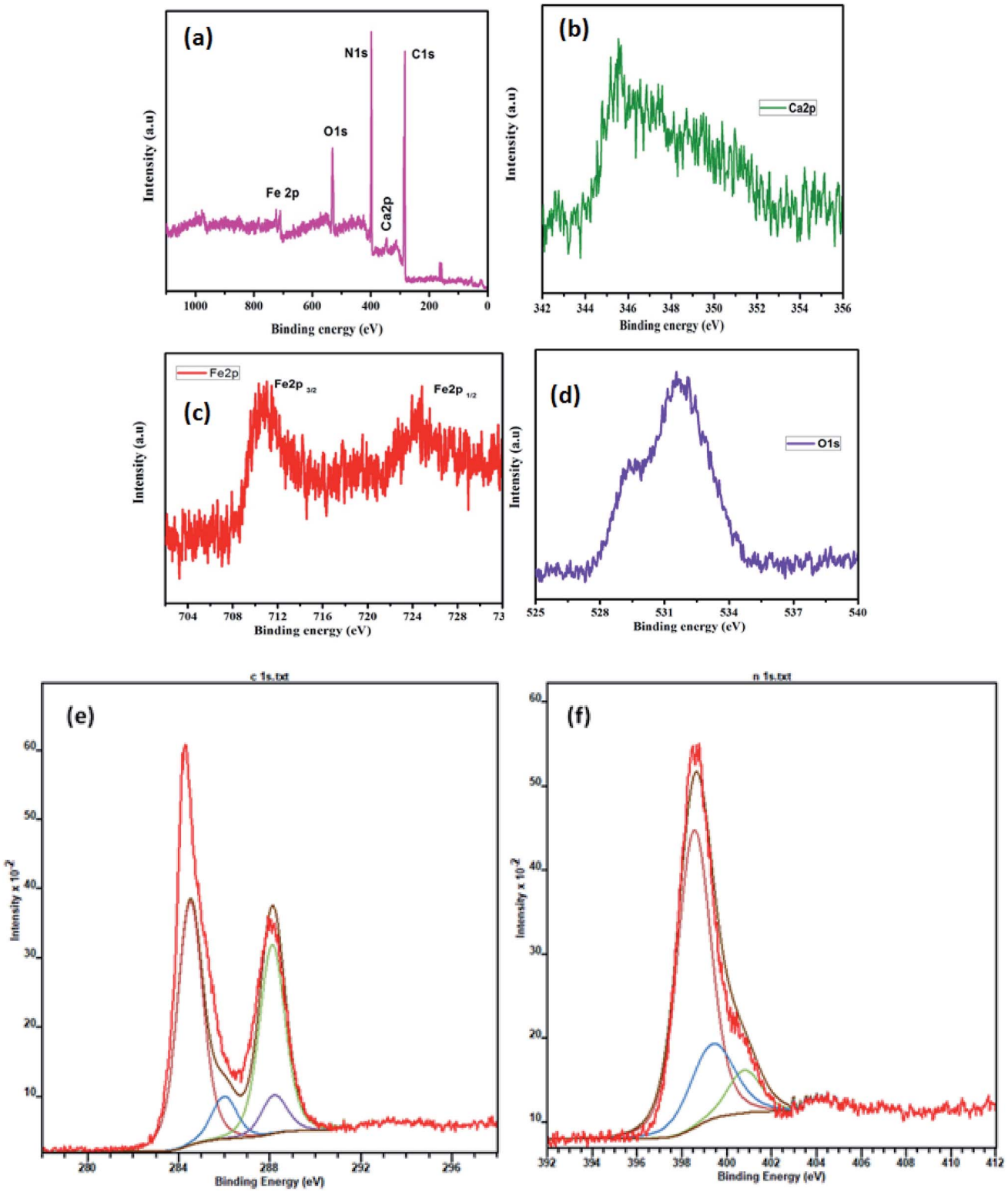

Fig. 7 XPS spectra of the as-prepared $CaFe_2O_4$/g-C_3N_4/CNT composite: (a) survey scan, (b) Ca 2p, (c) Fe 2p, (d) O 1s, (e) C 1s, and (f) N 1s.

it has a very high recombination rate. However, the PL intensity of the $CaFe_2O_4$/g-C_3N_4/CNT composite was remarkably compared with that of g-C_3N_4. The lower recombination rate in the photocatalytic system can be beneficial for the complete degradation of pollutions within a minimum time.[29]

The BET surface area and average pore size of $CaFe_2O_4$, g-C_3N_4, $CaFe_2O_4$/CNTs, and the $CaFe_2O_4$/g-C_3N_4/CNT nanocomposite were obtained from N_2 adsorption–desorption studies, as shown in Fig. 9. The N_2 adsorption–desorption curves of the prepared samples exhibit type IV isotherms,

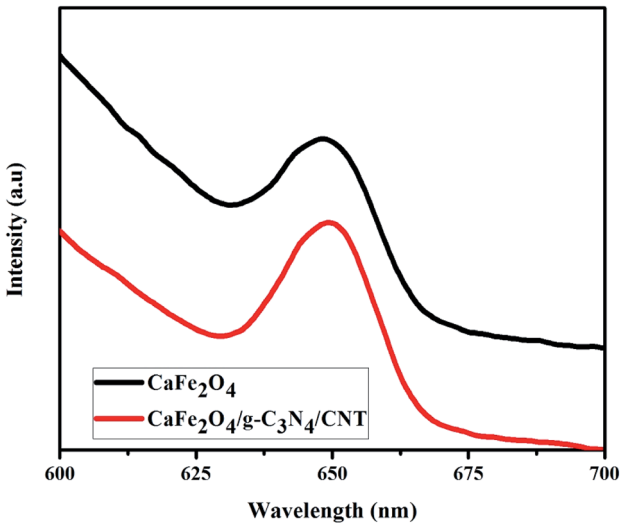

Fig. 8 PL analysis of $CaFe_2O_4$ and $CaFe_2O_4$/g-C_3N_4/CNTs composite.

indicating the pore size of the samples is mesoporous in nature using the BJH method. It was evident that the $CaFe_2O_4$/g-C_3N_4/CNTs photocatalyst exhibited the highest specific surface area, which is beneficial for higher photocatalytic activity.

The photogenerated charge carrier capability and separation nature of the composite were investigated by EIS measurements. Both $CaFe_2O_4$ and the $CaFe_2O_4$/g-C_3N_4/CNT composite exhibited semicircular Nyquist plots, but the diameter of the $CaFe_2O_4$/g-C_3N_4/CNT composite plot was smaller (Fig. 10), further confirming the faster interfacial charge transfer rate and outstanding separation rate of photogenerated charge carriers between g-C_3N_4 and $CaFe_2O_4$ due to the incorporation of CNT.

The spin-trapping ESR measurements were used to confirm the presence of active oxidation species produced over the $CaFe_2O_4$/g-C_3N_4/CNT composite during the photocatalytic process, and the results are shown in Fig. 11. Under visible light irradiation, the characteristic peaks of DMPO–$\cdot O_2^-$ and DMPO–$\cdot$OH were clearly observed, and the peak intensities were obvious when the irradiation time was increased up to 3 min. The ESR results confirmed that the $\cdot O_2^-$ and $\cdot$OH radicals were mainly generated during the photocatalytic process.

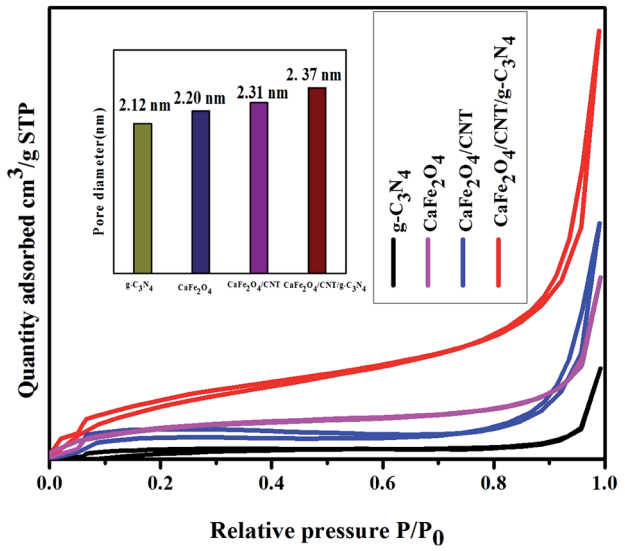

Fig. 9 BET analysis of $CaFe_2O_4$, g-C_3N_4, $CaFe_2O_4$//CNTs, and $CaFe_2O_4$/g-C_3N_4/CNT composite.

3.1. Photocatalytic activities and stability tests

The photocatalytic activity of g-C_3N_4, $CaFe_2O_4$, and $CaFe_2O_4$/g-C_3N_4/CNT composite for the visible light degradation of Cr(VI) and TC is shown in Fig. 12a. The photolysis of Cr(VI) and TC under visible light without photocatalysts was negligible. Using the pure g-C_3N_4 and $CaFe_2O_4$, the degradation rate was not appreciable due to their high recombination rate of charge carriers. Furthermore, using the binary systems of g-C_3N_4/CNT and $CaFe_2O_4$/CNT, the degradation rate of Cr(VI) and TC moderately increased. We found that the introduction of CNT in the g-C_3N_4/$CaFe_2O_4$ heterojunction enhanced the degradation rate for Cr and TC, and the best degradation efficiency was achieved upon the incorporation of CNT in the system, which confirms the importance of CNT in the ternary structure. The $CaFe_2O_4$/g-C_3N_4/CNT composite exhibited a photocatalytic efficiency of 97% (at 120 min) for the degradation of Cr(VI) and 98% (at 60 min) for TC under visible light (Fig. 13a). As show in Fig. 13b, the photodegradation rate of the $CaFe_2O_4$/g-C_3N_4/CNT composite decreased slightly after five reaction cycles, indicating the excellent reusability of the photocatalytic material. The role of pH strongly interferes with the photocatalytic removal of Cr(VI); thus, the effect of pH was also studied in the pH range of 3–9 with the $CaFe_2O_4$/g-C_3N_4/CNT composite. At a higher pH, the photocatalytic reduction rate for Cr(VI) was significantly reduced (Fig. 12b) due to the formation of $Cr_2O_7^{2-}$. At a lower pH value, Cr(VI) was easily removed due to the formation of $HCrO^{4-}$ and the protonated surface of the catalyst, which is more favorable the Cr(VI) removal.[30] Moreover, the reaction rate constant of the $CaFe_2O_4$/g-C_3N_4/CNTs ternary photocatalyst, as shown in Fig. 14, for the removal of Cr(VI) is 65 $\times 10^{-4}$ min^{-1} and removal of TC is 73 $\times 10^{-4}$ min^{-1}.

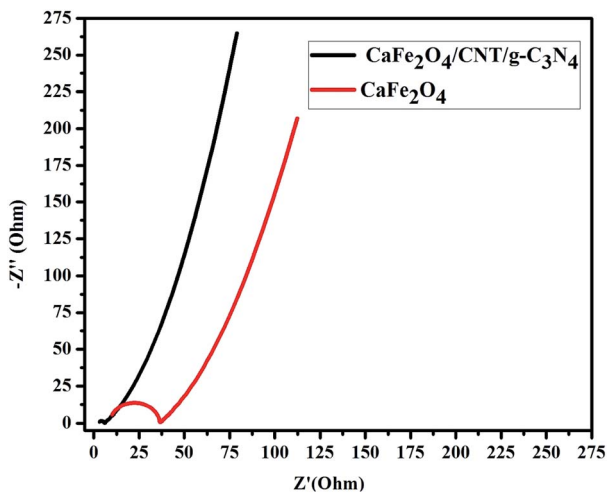

Fig. 10 EIS spectra $CaFe_2O_4$ and $CaFe_2O_4$/g-C_3N_4/CNT composite.

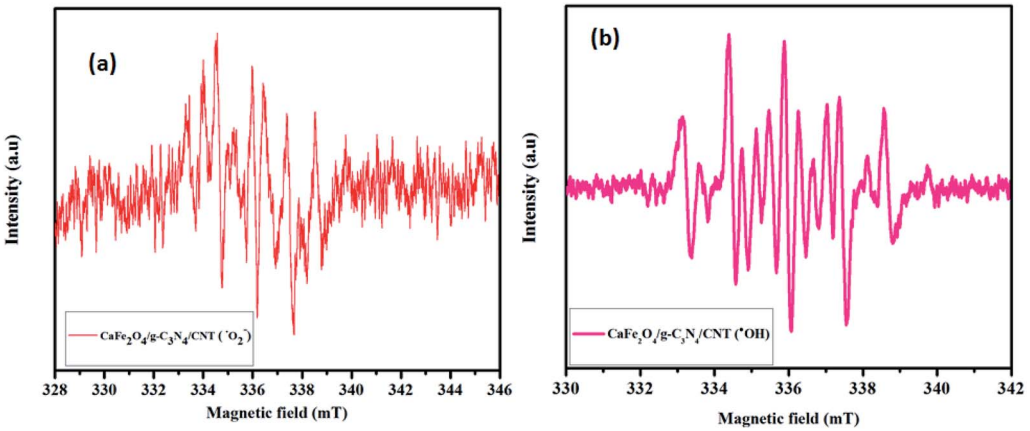

Fig. 11 EPR spectrum of $CaFe_2O_4/g\text{-}C_3N_4/CNT$ composite using DMPO.

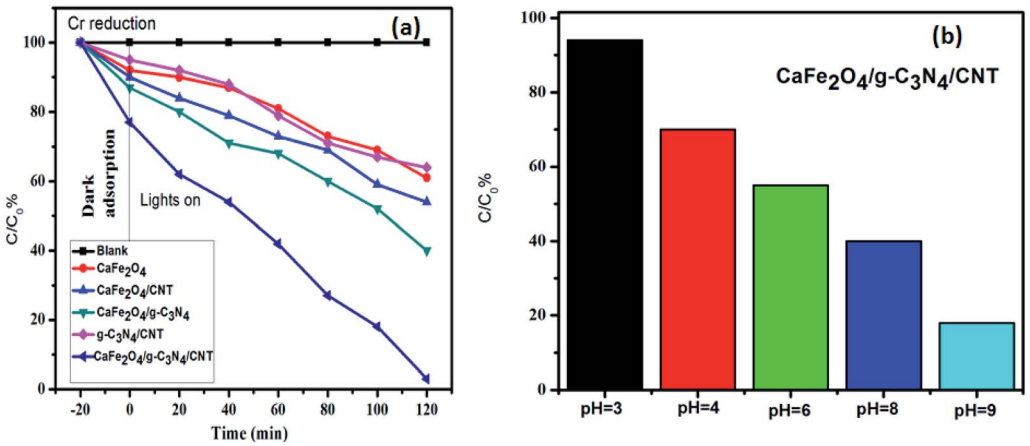

Fig. 12 (a) Adsorption and visible light photocatalytic performance of the samples for the degradation of Cr(VI) and (b) effect of pH on the removal of Cr(VI) using the $CaFe_2O_4/g\text{-}C_3N_4/CNTs$ composite.

3.2. Photocatalytic hydrogen production tests

In this work, the feasibility of using the $CaFe_2O_4/g\text{-}C_3N_4/CNT$ composite as a versatile photocatalyst for the production of hydrogen was studied. As shown in Fig. 15, the loading of CNT on $g\text{-}C_3N_4$ and $CaFe_2O_4$ resulted in a significant enhancement in the photocatalytic hydrogen production rate. Initially, with an increase in the loading of $g\text{-}C_3N_4$ in $CaFe_2O_4$, the hydrogen generation rate showed a remarkable improvement. In

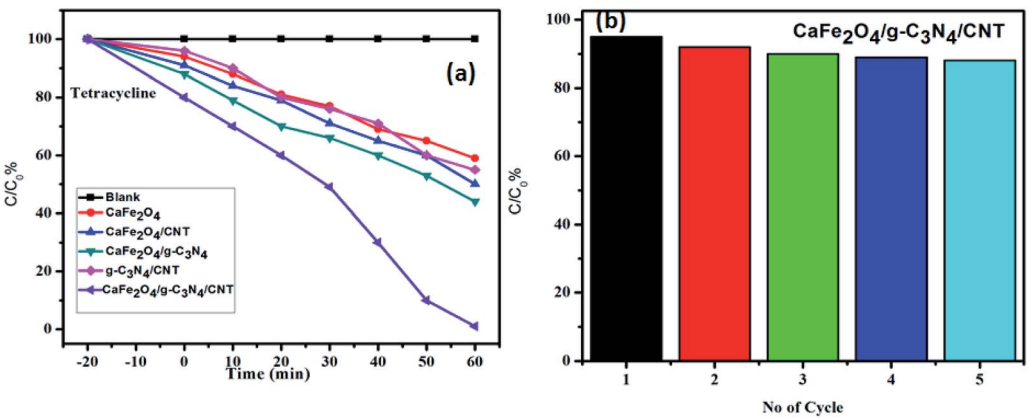

Fig. 13 (a) Adsorption and visible light photocatalytic performance of the samples in the degradation of TC and (b) stability test of the $CaFe_2O_4/g\text{-}C_3N_4/CNT$ composite in recycling degradation of TC.

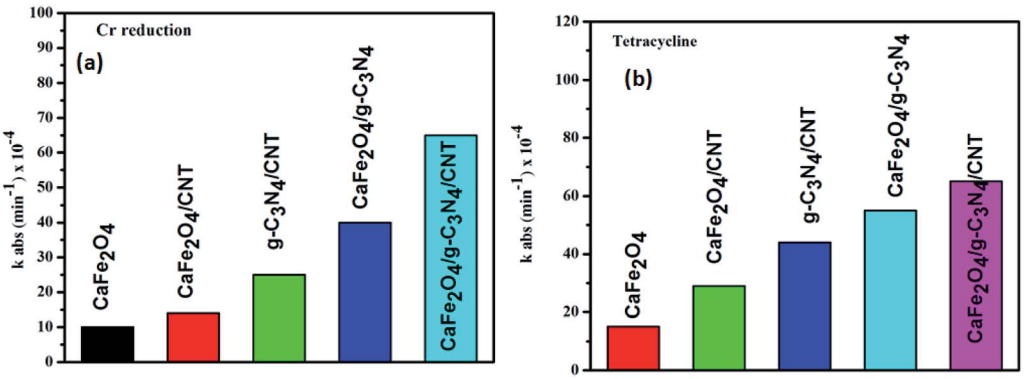

Fig. 14 Photodegradation kinetics of Cr and TC over the $CaFe_2O_4$/g-C_3N_4/CNT composite under visible light.

particular, the hydrogen generation rate of the $CaFe_2O_4$/g-C_3N_4/CNT composite sample increased to 1085 μmol h^{-1}, which is about nearly 3 times higher than that of bare $CaFe_2O_4$ (417 μmol h^{-1}). The AQY of $CaFe_2O_4$/g-C_3N_4/CNTs was calculated to be 7.2%. These results indicate that the CNT act as an effective co-catalyst for g-C_3N_4/$CaFe_2O_4$ and heterojunctions, and the loading ratio of CNT needs to be controlled within an appropriate range. Therefore, as a noble metal-free catalyst, $CaFe_2O_4$/g-C_3N_4/CNT composite can potentially be used as an economically feasible catalyst to replace precious metals such as Pt and Pd industrially to produce hydrogen. As shown in Fig. 16, to study the stability of the $CaFe_2O_4$/g-C_3N_4/CNT composite, cyclic runs for photocatalytic hydrogen production using the $CaFe_2O_4$/g-C_3N_4/CNT composite sample were performed. A slight decrease in the hydrogen production rate of the $CaFe_2O_4$/g-C_3N_4/CNT composite was observed in the last cycle, which confirms that the $CaFe_2O_4$/g-C_3N_4/CNT composite has excellent stability during the photocatalytic production of hydrogen besides the degradation reactions. Furthermore, the sample was collected after the cycle test and then characterized by XRD analysis. The XRD patterns of the reused catalyst exhibited no significant changes in the crystal structure after five consecutive cycles. Thus, the $CaFe_2O_4$/g-C_3N_4/CNT composite was determined to display good cyclic stability during the photocatalytic production of hydrogen.[31] Using all the characterization results, the plausible photocatalytic degradation mechanism with the $CaFe_2O_4$/g-C_3N_4/CNT composite for a high degradation rate and hydrogen production was proposed. Also, a comparison of the present work with previous reported catalysts is presented in Table 1.

3.3. Photocatalytic mechanisms

Under visible light illumination, both $CaFe_2O_4$ and g-C_3N_4 can be quickly excited to generate the corresponding photoinduced electrons and holes due to their moderate band gaps of 1.55 eV and 1.55 eV, respectively. Since the E_{CB} value of g-C_3N_4 (−1.15 eV)[32] is highly negative compared to that of $CaFe_2O_4$ (+1.57 eV), the ejected electrons towards the CB of g-C_3N_4 can be simply transferred to the CB of $CaFe_2O_4$. Meanwhile, the generated holes on the VB of $CaFe_2O_4$ may be transferred to the VB of g-C_3N_4 because the E_{VB} of $CaFe_2O_4$ (+1.98 eV) was more positive than that of g-C_3N_4 (+0.89 eV).[33] Furthermore, the additional impact of the CNT results in the transfer of more electron–hole pairs through the effective linkage, leading to an improvement in the lifetime of the carriers. In this mode, the charge separation of photogenerated electron–hole pairs can be drastically enhanced and the recombination rate can be minimized, thus

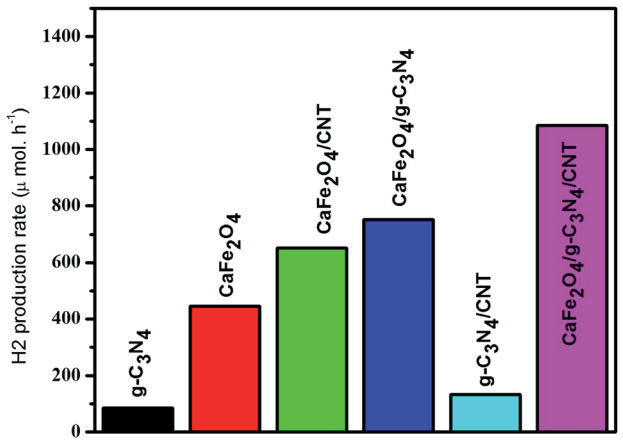

Fig. 15 Time-dependent photocatalytic hydrogen production rate of the $CaFe_2O_4$/g-C_3N_4/CNT composite under visible light.

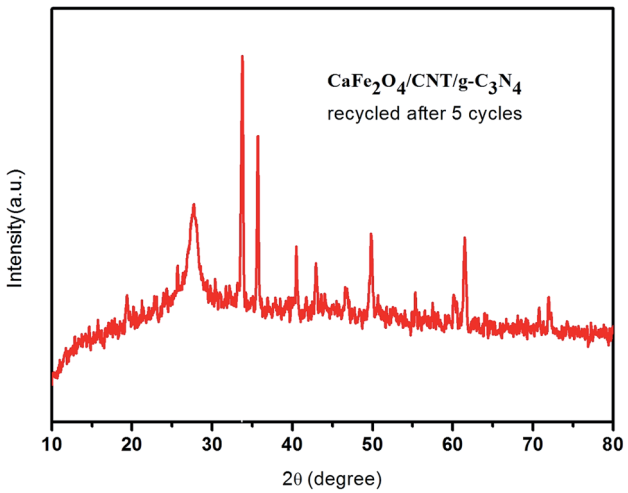

Fig. 16 XRD spectrum of the reused $CaFe_2O_4$/g-C_3N_4/CNT composite towards hydrogen production after three cycles.

Table 1 Catalytic, photocatalytic and post-illumination activities of different catalysts

Photocatalyst	Target pollutant	Irradiation time (min)	Decomposition (%)	Ref.
Biochar-coupled g-C_3N_4	Cr(VI)	300	100	41
TiO_2/g-C_3N_4@diatomite hybrid photocatalyst	Cr(VI)	300	100	42
N_2-g-C_3N_4 photocatalyst	Bisphenol-A	120	79	43
g-C_3N_4/Na-bentonite composites	Cr(VI) and RhB	120	88.6	44
0D/2D bismuth molybdate homojunction	Cr(VI)	80	100	45
AgI/$BiVO_4$ p–n junction photocatalyst	Tetracycline and Cr(VI)	100	70	46
$CaFe_2O_4$/g-C_3N_4/CNT composite	Tetracycline and Cr(VI)	120	98	This study

improving the photocatalytic ability of the $CaFe_2O_4$/g-C_3N_4/CNT composite.[34–40] The possible photocatalytic mechanism for the photodegradation of Cr(VI) and TC as well as hydrogen generation using the ternary $CaFe_2O_4$/g-C_3N_4/CNT composite under visible light irradiation is proposed in Fig. S1.†

4. Conclusion

In conclusion, we demonstrated a simple hydrothermal strategy for the fabrication of a ternary $CaFe_2O_4$/g-C_3N_4/CNT composite. The addition of CNT in the system outstandingly promoted the separation of photogenerated charge carriers. The as-synthesized $CaFe_2O_4$/g-C_3N_4/CNT composite exhibited improved light-harvesting capability, more proficient charge transfer capability and improved hydrogen production performance. The hydrogen production rate of the optimal $CaFe_2O_4$/g-C_3N_4/CNT composite was superior to that of pure $CaFe_2O_4$ and previous works. Furthermore, the optimal $CaFe_2O_4$/g-C_3N_4/CNT composite photocatalyst exhibited excellent performances for the photodegradation of Cr(VI) and TC with high stability. This work may inspire the development of rare earth- and noble metal-free catalysts for the degradation of pollutants and production of hydrogen in the near future.

Conflicts of interest

There are no conflicts of interest in this paper.

Acknowledgements

This work was sponsored by Scientific Research Starting Fund from Shengli College China University of Petroleum (KQ2019-007), Shandong Postdoctoral Innovation Talent Support Program, Project of Shandong Province Higher Educational Science and Technology Program, Training Program of Innovation for Undergraduates (2019001).

References

1 F. Chang, Y. Xie, C. Li, J. Chen, J. Luo, X. Hu and J. Shen, A facile modification of g-C_3N_4 with enhanced photocatalytic activity for degradation of methylene blue, *Appl. Surf. Sci.*, 2013, **280**, 967–974.

2 Y. Xia, Q. Li, X. Wu, K. Lv, D. Tang and M. Li, Facile synthesis of CNTs/$CaIn_2S_4$ composites with enhanced visible-light photocatalytic performance, *Appl. Surf. Sci.*, 2017, **391**, 565–571.

3 Y. Choi, M. S. Koo, A. D. Bokare, D. H. Kim, D. W. Bahnemann and W. Choi, Sequential process combination of photocatalytic oxidation and dark reduction for the removal of organic pollutants and Cr(VI) using Ag/TiO_2, *Environ. Sci. Technol.*, 2017, **51**, 3973–3981.

4 A. Y. Meng, B. C. Zhu, B. Zhong, L. Y. Zhang and B. Cheng, Direct Z-scheme TiO_2/CdS hierarchical photocatalyst for enhanced photocatalytic H_2-production activity, *Appl. Surf. Sci.*, 2017, **422**, 518–527.

5 X. Zhang, S. Cao, Z. Wu, S. Zhao and L. Piao, Enhanced photocatalytic activity towards degradation and H_2 evolution over one dimensional TiO_2@MWCNTs heterojunction, *Appl. Surf. Sci.*, 2017, **402**, 360–368.

6 G. Liu, G. Zhao, W. Zhou, Y. Liu, H. Pang, H. Zhang, D. Hao, X. Meng, P. Li, T. Kako and J. Ye, In situ bond modulation of graphitic carbon nitride to construct p-n homojunctions for enhanced photocatalytic hydrogen production, *Adv. Funct. Mater.*, 2016, **26**, 6822–6829.

7 S. Chidambaram, A. Vijay, G. Mohan Kumar, M. Alagiri, J. Thiruvadigal and M. Rathinam, Three-dimensional (3D) flower-like nanoarchitectures of ZnO-Au on MWCNTs for visible light photocatalytic applications, *Appl. Surf. Sci.*, 2018, **449**, 631–637.

8 A. Payan, M. Fattahi, S. Jorfib, B. Roozbehani and S. Payan, Synthesis and characterization of titanate nanotube/single-walled carbon nanotube (TNT/SWCNT) porous nanocomposite and its photocatalytic activity on 4-chlorophenol degradation under UV and solar irradiation, *Appl. Surf. Sci.*, 2018, **434**, 336–350.

9 J. Wang, X. Xu, F. Cao, Y. Wang, S. Li and G. Qin, In situ fabrication of α-Fe_2O_3/$CaFe_2O_4$ p-n heterojunction with enhanced VOCs photodegradation activity, *Adv. Powder Technol.*, 2019, **30**, 590–595.

10 M. Li, H. Y. Bai, Z. L. Da, X. Yan, C. Chen, J. H. Jiang, W. Q. Fan and W. D. Shi, Electrospinning synthesis and photocatalytic property of $CaFe_2O_4$/$MgFe_2O_4$ heterostructure for degradation of tetracycline, *Cryst. Res. Technol.*, 2015, **50**, 244–249.

11 Y. K. Luo, Synthesis and characterization of novel $CaFe_2O_4$/Bi_2O_3 composite photocatalysts, *Mater. Lett.*, 2018, **225**, 17–20.

12 X. Liu, Y. H. Zhang, Y. S. Jia, J. Z. Jiang, Y. B. Wang, X. S. Chen and T. Gui, Visible light-responsive carbon-

decorated p-type semiconductor $CaFe_2O_4$ nanorod photocatalyst for efficient remediation of organic pollutants, *Chin. J. Catal.*, 2017, **38**, 1770.

13 R. C. Pawar, S. Kang, S. H. Ahn and C. S. Lee, Gold nanoparticle modified graphitic carbon nitride/multi-walled carbon nanotube (g-C_3N_4/CNT/Au) hybrid photocatalysts for effective water splitting and degradation, *RSC Adv.*, 2015, **5**, 24281–24292.

14 D. Chaudhary, V. D. Vankar and N. Khare, Noble metal free g-C_3N_4/TiO_2/CNT ternary nanocomposite with enhanced photocatalytic performance under visible light irradiation with multi-step charge transfer process, *Sol. Energy*, 2017, **158**, 132–139.

15 Y. Bao and K. Chen, Novel Z-scheme BiOBr/reduced graphene oxide/protonated g-C_3N_4 photocatalyst: synthesis, characterization, visible light photocatalytic activity and mechanism, *Appl. Surf. Sci.*, 2018, **437**, 51–61.

16 G. Mamba and A. K. Mishra, Graphitic carbon nitride (g-C_3N_4) nanocomposites: a new and exciting generation of visible light driven photocatalysts for environmental pollution remediation, *Appl. Catal., B*, 2016, **198**, 347–377.

17 S. Vadivel, D. Maruthamani, A. Habibi-Yangjeh, B. Paul, S. S. Dhar and K. Selvam, Facile synthesis of novel $CaFe_2O_4$/g-C_3N_4 nanocomposites for degradation of methylene blue under visible-light irradiation, *J. Colloid Interface Sci.*, 2016, **480**, 126–136.

18 Y. K. Kim and H. Park, Light-harvesting multi-walled carbon nanotubes and CdS hybrids: application to photocatalytic hydrogen production from water, *Energy Environ. Sci.*, 2011, **4**, 685–694.

19 Y. X. Zhang, D. Ma, J. Wu, Q. Z. Zhang, Y. J. Xin and N. Bao, One-step preparation of CNTs/$InVO_4$ hollow nanofibers by electrospinning and its photocatalytic performance under visible light, *Appl. Surf. Sci.*, 2015, **353**, 1260–1268.

20 A. Doi, M. Nomura, Y. Obukuro, R. Maeda and K. Obata, Characterization of Ti doped $CaFe_2O_4$ prepared from a malic acid complex, *J. Ceram. Soc. Jpn.*, 2014, **122**, 175–178.

21 H. Q. Wang, J. Z. Li, M. J. Zhou, Q. F. Guan, Z. Y. Lu, P. W. Huo and Y. S. Yan, Preparation and characterization of Ag_2O/SWNTs photocatalysts and its photodegradation on tetracycline, *J. Ind. Eng. Chem.*, 2015, **30**, 64–70.

22 X. J. She, J. Wu, H. Xu, J. Zhong, Y. Wang, Y. H. Song, K. Nie, Y. Liu, Y. Yang, M.-T. F. Rodrigues, R. Vajtai, J. Lou, D. Du, H. Li and P. M. Ajayan, High efficiency photocatalytic water splitting using 2D α-Fe_2O_3/g-C_3N_4 Z-scheme catalysts, *Adv. Energy Mater.*, 2017, **7**, 1700025.

23 X. W. Zhu, J. Y. Liu, Z. Z. Zhao, J. Yan, Y. G. Xu, Y. H. Song, H. Y. Ji, H. Xu and H. M. Li, Hydrothermal synthesis of mpg-C_3N_4 and Bi_2WO_6 nest-like structure nanohybrids with enhanced visible light photocatalytic activities, *RSC Adv.*, 2017, **7**, 38682–38690.

24 N. K. Veldurthi, N. K. Eswar, S. A. Singh and G. Madras, Cooperative effect between $BaTiO_3$ and $CaFe_2O_4$ in a cocatalyst-free heterojunction composite for improved photochemical H_2 generation, *Int. J. Hydrogen Energy*, 2018, **43**, 22929–22941.

25 T. Yamashita and P. Hayes, Analysis of XPS spectra of Fe2p and Fe3p ions in oxide materials, *Appl. Surf. Sci.*, 2008, **254**, 2441–2449.

26 X. Yang, D. Li, Z. H. Ren, R. G. Zeng, S. Y. Gong and D. K. Zhou, Colossal dielectric performance of pure barium titanate ceramics consolidated by spark plasma sintering, *RSC Adv.*, 2016, **6**, 75422–75429.

27 J. H. Liu, T. K. Zhang, Z. C. Wang, G. Dawson and W. Chen, Simple pyrolysis of urea into graphitic carbon nitride with recyclable adsorption and photocatalytic activity, *J. Mater. Chem.*, 2011, **21**, 14398–14401.

28 W. J. Shan, Y. Hu, Z. G. Bai, M. M. Zheng and C. H. Wei, In situ preparation of g-C_3N_4/bismuth-based oxide nanocomposites with enhanced photocatalytic activity, *Appl. Catal., B*, 2016, **188**, 1–12.

29 L. Liu, Y. H. Qi, J. R. Lu, S. L. Lin, W. J. An, Y. H. Liang and W. Q. Cui, A stable Ag_3PO_4@gC_3N_4 hybrid core@shell composite with enhanced visible light photocatalytic degradation, *Appl. Catal., B*, 2016, **183**, 133–141.

30 D. Xiao, K. Dai, Y. Qu, Y. Yin and H. Chen, Hydrothermal synthesis of α-Fe_2O_3/g-C_3N_4 composite and its efficient photocatalytic reduction of Cr(VI) under visible light, *Appl. Surf. Sci.*, 2015, **358**, 181–187.

31 L. Ge, C. Han and J. Liu, Novel visible light-induced g-C_3N_4/Bi_2WO_6 composite photocatalysts for efficient degradation of methyl orange, *Appl. Catal., B*, 2011, **108–109**, 100–107.

32 C. Han, Novel visible light induced Co_3O_4/g-C_3N_4 heterojunction photocatalysts for efficient degradation of methyl orange, *Appl. Catal., B*, 2014, **147**, 546–553.

33 C. Shifu, Z. Wei, L. Wei, Z. Huaye and Y. Xiaoling, Preparation, characterization and activity evaluation of p–n junction photocatalyst p-$CaFe_2O_4$/n-ZnO, *Chem. Eng. J.*, 2009, **155**, 466–473.

34 D. K. Padhi and K. Parida, Facile fabrication of, α-FeOOH, nanorod/RGO, composite: a robust photocatalyst for reduction of Cr(VI), *J. Mater. Chem. A*, 2014, **2**, 10300–10312.

35 X. Li, J. Yu, M. Jaroniec and X. Chen, Co catalysts for Selective Photoreduction of CO_2 into Solar Fuels, *Chem. Rev.*, 2019, **119**(6), 3962–4179.

36 X. Li, J. Xie, C. Jiang, J. Yu and P. Zhang, Review on design and evaluation of environmental photocatalysts, *Front. Environ. Sci. Eng.*, 2018, **12**, 14.

37 J. Wen, J. Xie, X. Chen and X. Li, A review on g-C_3N_4-based photocatalysts, *Appl. Surf. Sci.*, 2017, **391**, 72–123.

38 R. Shen, J. Xie, Y. Ding, S. Liu, A. Adamski, X. Chen and X. Li, Carbon Nanotube-Supported Cu_3P as High-Efficiency and Low-Cost Cocatalysts for Exceptional Semiconductor-Free Photocatalytic H_2 Evolution, *ACS Sustainable Chem. Eng.*, 2019, **7**(3), 3243–3250.

39 R. Shen, J. Xie, Q. Xiang, X. Chen, J. Jiang and X. Li, Ni-based photocatalytic H_2-production cocatalysts, Chinese, *J. Catal.*, 2019, **40**(3), 240–288.

40 Z. Li, Y. Ma, X. Hu and E. L. J. Fan, Enhanced photocatalytic H_2 production over dual-cocatalyst-modified g-C_3N_4 heterojunctions, Chinese, *J. Catal.*, 2019, **40**, 434–445.

41 K. Li, Z. Huang, S. Zhu, S. Luo, L. Yan, Y. Dai, Y. Guo and Y. Yang, Removal of Cr(VI) from water by a biochar-

coupled g-C_3N_4 nanosheets composite and performance of a recycled photocatalyst in single and combined pollution systems, *Appl. Catal., B*, 2019, **243**, 386–396.

42 Q. Sun, X. Hu, S. Zheng, J. Zhang and J. Sheng, Effect of calcination on structure and photocatalytic property of N-TiO_2/g-C_3N_4@diatomite hybrid photocatalyst for improving reduction of Cr(VI), *Environ. Pollut.*, 2019, **245**, 53–62.

43 H. Wang, Q. Li, S. Zhang, Z. Chen, W. Wang, G. Zhao, L. Zhuang, B. Hu and X. Wang, Visible-light-driven N_2-g-C_3N_4 as a highly stable and efficient photocatalyst for bisphenol A and Cr(VI) removal in binary systems, *Catal. Today*, 2019, **335**, 110–116.

44 Y. Guo, C. Li, Y. Guo, X. Wang and X. Li, Ultrasonic-assisted synthesis of mesoporous g-C_3N_4/Na-bentonite composites and its application for efficient photocatalytic simultaneous removal of Cr(VI) and RhB, *Colloids Surf., A*, 2019, **578**, 12362.

45 J. Xua, J. Yue, J. Niu and M. Chen, Synergistic removal of Cr(VI) and dye contaminants by 0D/2D bismuth molybdate homojunction photocatalyst under visible light, *Appl. Surf. Sci.*, 2019, **484**, 1080–1088.

46 W. Zhao, J. Li, B. Dai, Z. Cheng, J. Xu, K. Ma, L. Zhanga, N. Shenge, G. Mao, H. Wud, K. Wei and D. Y. C. Leung, Simultaneous removal of tetracycline and Cr(VI) by a novel three dimensional AgI/$BiVO_4$ p-n junction photocatalyst and insight into the photocatalytic mechanism, *Chem. Eng. J.*, 2019, **369**, 716–725.